Multi-scale magnetic coupling of Fe@SiO_2@C-Ni yolk@triple-shell microsphere for broadband microwave absorption

*Xiaofeng Shi, Wenbin You, Yunhao Zhao, Xiao Li, Zhengzhong Shao and Renchao Che**

Laboratory of Advanced Materials, Department of Materials Science and Collaborative Innovation Center of Chemistry for Energy Materials (iChem), Fudan University, Shanghai 200438, P. R. China

* E-mail: rcche@fudan.edu.cn

S1: The details of conventional electromagnetic measurements

The as-prepared Fe@SiO_2@C-Ni samples were mixed homogeneously with the wax in a mass ratio of 7:3. The mixture was compressed into a columnar ring of 7.00 mm outer diameter and 3.00 mm inner diameter. The complex relative permittivity and permeability were measured by an N5230C vector network analyzer in the 2-18 GHz range.

S2: **More discussion about Electron holography**

Off-axis electron holography is an outstanding technique that can obtain the quantitative information on the electrostatic and magnetic field of the measured sample under nano-scale resolution. The phase information is presented in one dimension without regard to dynamical diffraction effects by

$$\phi(x) = \left(\frac{2\pi}{\lambda}\right)\left(\frac{E + E_0}{E(E + 2E_0)}\right)\int V(x,z)\mathrm{d}z - \left(\frac{e}{\hbar}\right) \times \iint B_{\perp}(x,z)\mathrm{d}x\mathrm{d}z$$

Where z is the incident beam direction, x is a direction in the plane of the sample, $B\perp$ is the magnetic induction perpendicular to the x and z, V is the mean inner potential, λ is the wavelength, E and E0 are the kinetic and rest mass energies of the incident electron, respectively.

The plane electron wave pass through the sample, which carries the amplitude and phase information of sample. In the process of experiment, from the Fourier transform of the hologram, the appropriate sideband position is selected to carry out the inverse Fourier transform, and the amplitude and phase information are calculated. In this paper, the electron holographic reconstruction map shows the stray magnetic field lines out of the magnetic microsphere.

S3: **The analysis of FTIR spectrum**

Fourier transform infrared (FT-IR) is employed to measure the compositions of the sample. The characteristic peaks at 1074 cm^{-1}, 943 cm^{-1}, 805 cm^{-1} and 464 cm^{-1} correspond to the Si-O-Si, Si-O-H stretching vibrations and bending vibration of O-Si-O, respectively, which shows the existence of SiO_2. Peaks at 1283−1429 cm^{-1} are attributed to C−OH stretching and O−H bending vibrations. The peak at 1620 cm^{-1} is assigned to C=C vibrations, which reflects the carbon species on the FSCN microsphere surface from carbonated PDA. No peaks are observed at ~500-600 cm^{-1}, indicating the inexistence of Fe-O or Ni-O.

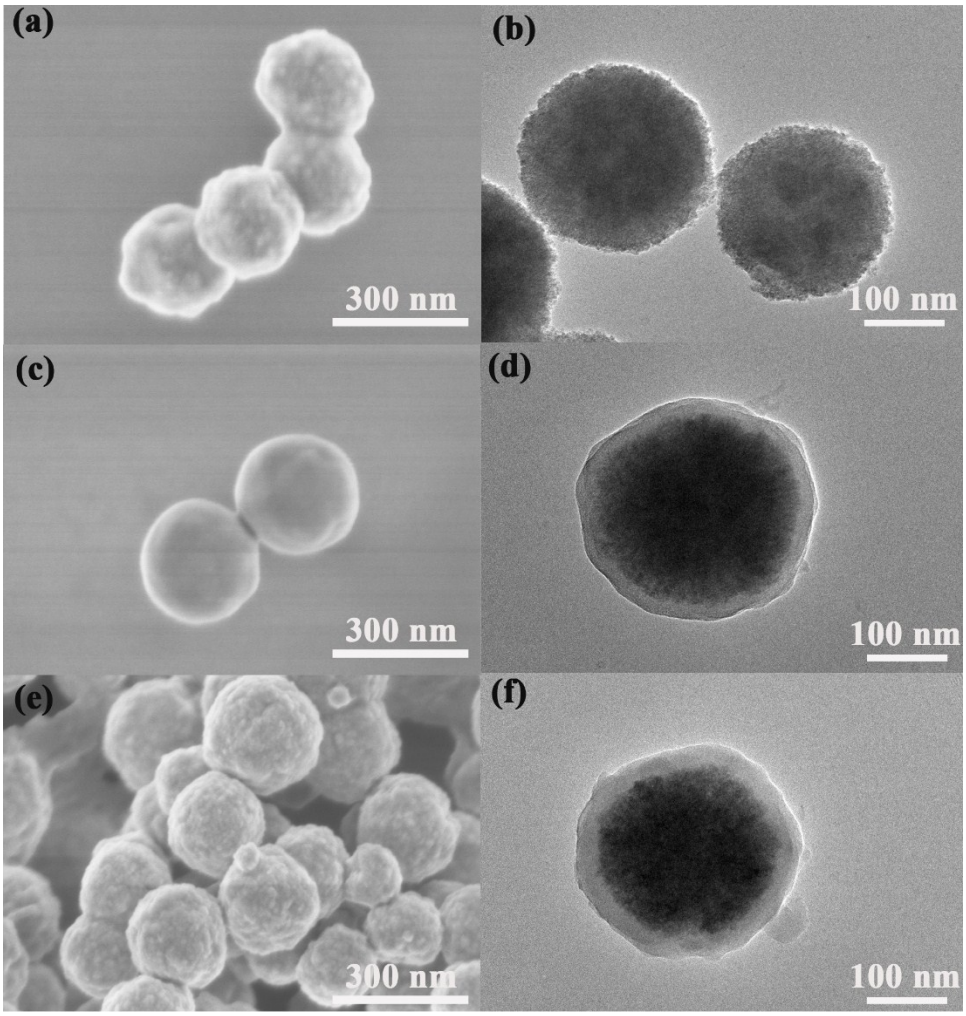

Figure S1. The SEM and TEM images of Fe_3O_4, Fe_3O_4@SiO_2 and Fe_3O_4@SiO_2@PDA-Ni^{2+}

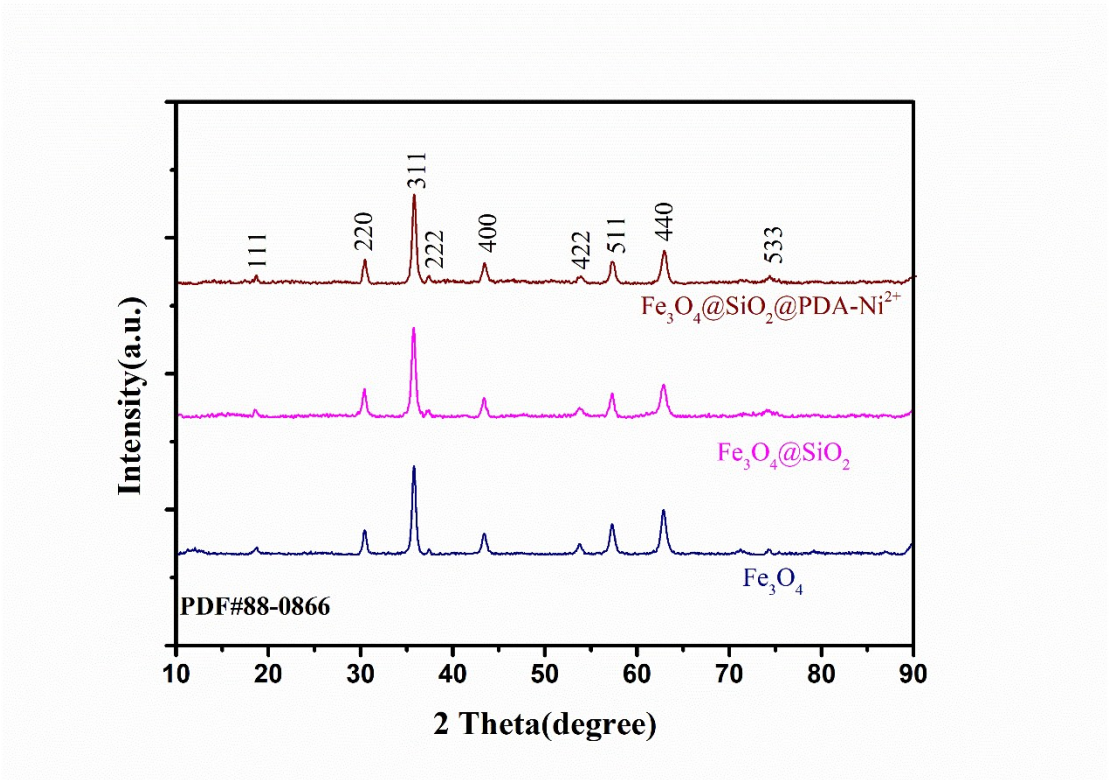

Figure S2. XRD patterns of Fe_3O_4, Fe_3O_4@SiO_2 and Fe_3O_4@SiO_2@PDA-Ni^{2+}

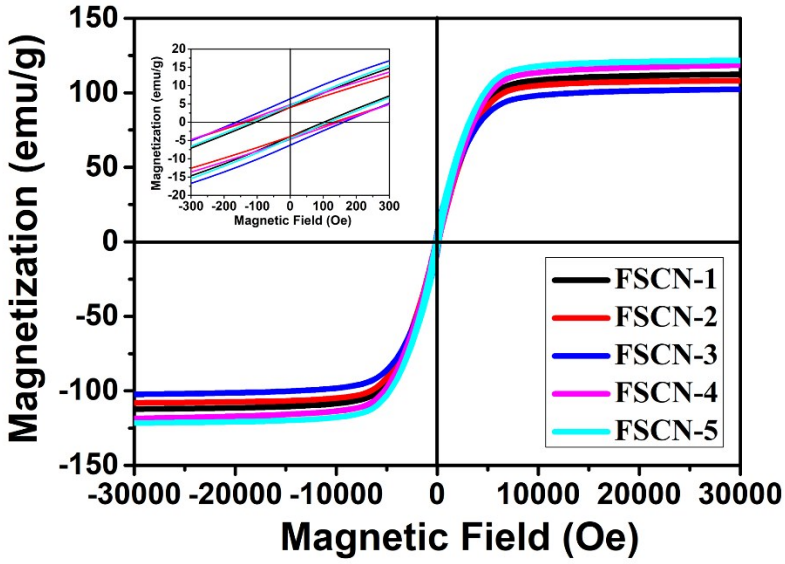

Figure S3. Hysteresis loops of FSCN series measured at 300K, The inset gives an enlarged view of the hysteresis loops (−300 to 300 Oe).

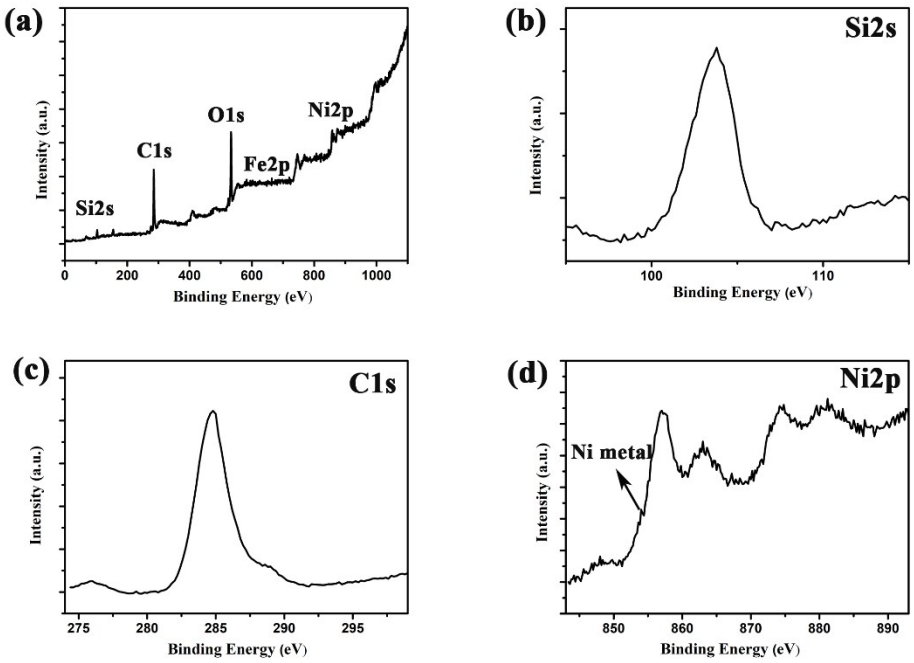

Figure S4. XPS spectra **of** Fe@SiO_2@C-Ni microsphere.

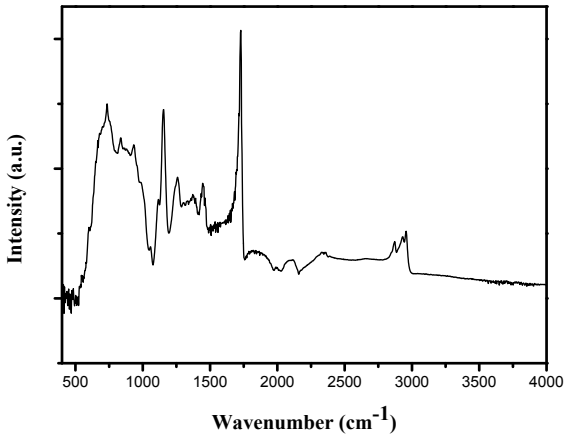

Figure S5. FTIR spectrum **of** Fe@SiO_2@C-Ni microsphere.

Table S1 MA performance of traditional absorbents in previous references and this work

Sample	Optimal RL (dB)	Frequency range (GHz) (RL < –10dB)	References
Fe_3O_4@SnO_2	-22.6	10.0-12.2	[1]

Fe_3O_4@TiO_2	-33.4	4.3-12.1	[2]
Fe_3O_4@C	-20.6	11.8-15.6	[3]
FeCo/C/$BaTiO_3$	-41.7	9.4-14.5	[4]
γ-Fe_2O_3@ C@ α-MnO_2	-41.7	7.48-16.66	[5]
CoNi@SiO_2@TiO_2	-58.2	7.7-13.2	[6]
Fe_3O_4@MnO_2	-48.5	7.4-13.8	[7]
NiO@graphene	-59.6	12.84-16.72	[8]
CoNi@ SiO_2@C	-46.0	7.1-12.7	[9]
Fe_3O_4@SiO_2@RGO	-26.6	8.4-11.8	[10]
Co/CNTs	-49.16	12.4-16.6	[11]
Fe_3O_4/PANI	-24.3	11.04-15.68	[12]
Fe_3O_4@ppy	−31.5	12.8–18	[13]
CoNi@C	−25	12–18	[14]
NiO @SiO_2@graphene	−43.8	9.2-15	[15]
This work	-45.5	9.8-18	herein

1. Y.-J. Chen, P. Gao, R.-X. Wang, C.-L. Zhu, L.-J. Wang, M.-S. Cao and H.-B. Jin, *The Journal of Physical Chemistry C*, 2009, **113**, 10061-10064.
2. J. Liu, J. Xu, R. Che, H. Chen, M. Liu and Z. Liu, *Chemistry–A European Journal*, 2013, **19**, 6746-6752.
3. Y. Du, W. Liu, R. Qiang, Y. Wang, X. Han, J. Ma and P. Xu, *ACS applied materials & interfaces*, 2014, **6**, 12997-13006.
4. J. Jiang, D. Li, D. Geng, J. An, J. He, W. Liu and Z. Zhang, *Nanoscale*, 2014, **6**, 3967-3971.
5. W. You, H. Bi, W. She, Y. Zhang and R. Che, *Small*, 2017, **13**, 1602779.
6. Q. Liu, Q. Cao, H. Bi, C. Liang, K. Yuan, W. She, Y. Yang and R. Che, *Advanced Materials*, 2016, **28**, 486-490.
7. M. Qiao, X. Lei, Y. Ma, L. Tian, K. Su and Q. Zhang, *Chemical Engineering Journal*, 2016, **304**, 552-562.
8. L. Wang, H. Xing, S. Gao, X. Ji and Z. Shen, *Journal of Materials Chemistry C*, 2017, **5**, 2005-2014.

9. S. Zhou, Y. Huang, X. Liu, J. Yan and X. Feng, *Industrial & Engineering Chemistry Research*, 2018, **57**, 5507-5516.
10. Y.-F. Pan, G.-S. Wang and Y.-H. Yue, *RSC Advances*, 2015, **5**, 71718-71723.
11. X. Xiao, Z. Tan, W. Tian, Y. Guo, H. Wang, J. Fu and X. Jian, *Composites Part B: Engineering*, 2018, **152**, 316-323.
12. J. Hou, L. Zhang, H. Qiu, W. Duan, X. Wang, X. Wan and X. Du, *Journal of Materials Science: Materials in Electronics*, 2017, **28**, 9279-9288.
13. M.Qiao, x. Lei, Y. Ma, L. Tian, K. Su and Q. Zhang, *Industrial & Engineering Chemistry Research*, 2016,55, 6263-6275.
14. H. Wang, Y. Dai, W. Gong, D. Geng, S. Ma, D. Li, W. Liu and Z. Zhang, *Applied Physics Letters*, 2013, 102, 223113.
15. L. Wang, Y. Huang, X. Ding, P. Liu and M. Zong, *RSC Advances*, 2013, 3, 23290-23295.